Pressure-induced superconductivity in the hydrogen-rich pseudobinary CaB-H$_n$ compounds

Wen-Hua Yang,[1] Wen-Cai Lu,[1,2,*] Wei Qin,[1] Hui-Juan Sun,[1] Xu-Yan Xue,[1] K. M. Ho,[3] and C. Z. Wang[3,†]

[1]*College of Physics, Qingdao University, Qingdao, Shandong 266071, People's Republic of China*

[2]*Institute of Theoretical Chemistry, Jilin University, Changchun, Jilin 130021, People's Republic of China*

[3]*Ames Laboratory-U.S. DOE and Department of Physics and Astronomy, Iowa State University, Ames, Iowa 50011, USA*

(Received 6 July 2021; revised 23 October 2021; accepted 1 November 2021; published 15 November 2021)

The crystal structures of CaB-H$_n$ compounds with $n = 1$–12 in a pressure range of 50–300 GPa were studied using the genetic algorithm method and first-principles density-function theory calculations. Stable structures with stoichiometry of $CaBH_6$ and $CaBH_7$ were predicted in different pressure range. BH_4, BH_5, and BH_6 units were found to be the main motifs in these compounds. Moreover, metastable $Imm2$ $CaBH_7$ is dynamically stable above 180 GPa, with the formation of tetrahedral BH_4 unit surrounded by Ca atom and H_3 unit. Electron-phonon coupling (EPC) calculations reveal that the superconducting properties are closely related to the strong hydrogen-boron bonding of the BH_4 unit in $Imm2$, and T_c can reach ~200 K at 200 GPa. As the major units, BH_4, BH_5, and BH_6 units exist in the $Imm2$, P_2, and $P2_1/m$ phases of $CaBH_7$ at 300 GPa, respectively; the corresponding EPC parameter λ decreases with the increase of hydrogen content in $CaBH_7$.

DOI: 10.1103/PhysRevB.104.174106

I. INTRODUCTION

Due to its high Debye temperature and strong electron-phonon coupling, high-pressure metallic phase of hydrogen is considered a potential high-temperature superconductor. However, hydrogen is expected to metallize around 450 GPa which is difficult to achieve at the current laboratory conditions [1]. Hydrogen-rich compounds can become metallic and superconducting at lower pressures in comparison with pure hydrogen phases [2], because of "chemical compression." A recent breakthrough in the discovery of superconducting hydrogen-rich compounds is the observation of high-temperature superconductivity ($T_c \sim 287$ K) in carbonaceous sulfur hydride compounds under high pressure (267 GPa) [3]. A high T_c of about 200 K at a pressure of 200 GPa has also been predicted for hydrogen sulfides and confirmed by experiments [4–6]. Drozdov *et al.* [7] have also synthesized lanthanum hydride by laser heating to lanthanum in hydrogen atmosphere under 170 GPa, and showed that LaH_{10} has superconducting behavior at 250 K at 170 GPa. Evidence for superconductivity above 260 K in lanthanum superhydride at 180–200 GPa was also reported by Somayazulu *et al.* [8]. Moreover, CaH_6, MgH_6, YH_{10}, and LaH_{10}, have been predicted to have possible high-T_c superconductivity in the range 235–326 K at the pressure of 150–300 GPa [9–12].

While binary hydrides have been investigated intensively by experimental synthesis and computational predictions, structures and superconductivity of ternary hydrides have also attracted considerable attention [13–20]. We note that ternary compounds containing both hydrogen and boron elements have also been studied [21–23]. HBS [21] is shown to be stable above 25 GPa. It exhibits diverse phases from semiconductor to metal as the pressure increases, and becomes superconductor with a T_c of 0.8 and 1.9 K at 300 and 400 GPa, respectively. Due to strong hydrogen-boron bonding, metallic Li_2BH_6 [22] displays a critical superconducting temperature T_c of ~100 K between 100 and 200 GPa. Recently, theoretical investigations have also been devoted to exploring the superconducting properties in ternary La-B-H compounds [24–26]. These studies made significant progress in searching for superconductors at high pressure. In particular, Ref. [25] showed that a H-rich $LaBH_8$ with an $Fm\bar{3}m$ symmetry exhibits an estimated superconducting T_c of 156 K at 55 GPa. It also showed that B–H bond is stronger than that of H–H in this structure, and the B atoms accommodate all the H atoms to form BH_8 units.

In addition to the hydride compounds discussed above, compounds containing Ca and B have also been investigated for possible superconductivity. At ambient pressure, simple hexagonal CaB_2 structure, which exhibits a high density of states at the Fermi level, is predicted to be a superconductor with a T_c of 50 K [27]. *Imma* CaB with a zigzag boron chain was predicted to be a superconductor with a T_c of ~6 K at 20 GPa [27]. It is also interesting to note that both Ca atom and B atom can form stable hydrides, respectively. Ca-H and B-H compounds have also attracted a great deal of attention in the research for superconducting materials [10,28–32]. For example, crystal structure of B_2H_6 with a *pbcn* symmetry becomes a superconductor with a T_c of 125 K at high pressure (360 GPa) [28]. CaH_6 with the H-clathrate structure was predicted to have a T_c of 235 K at 150 GPa [10]. Recently, calcium borohydrides have been investigated under the high pressure. $Pa\bar{3}$ $CaBH_6$ and Pm $Ca_2B_2H_{13}$ were predicted to have the T_c of 119 and 89 K, respectively, at 300 GPa [33].

Considering that higher hydrogen content in many hydride compounds was predicted to give higher T_c values and Ca-B

*wencailu@jlu.edu.cn

†wangcz@ameslab.gov

compounds also exhibit superconductivity, in this paper, we performed an extensive structural search for H-rich CaB-H_n ternary compounds with $n = 1$–12 in a pressure range of 50–300 GPa. The results showed that CaB-H_n with odd-H stoichiometry (e.g., $CaBH_7$, $CaBH_9$, and $CaBH_{11}$) is more stable. $CaBH_6$ and $CaBH_8$ are the stable compounds with the even-H stoichiometry. BH_3, BH_4, BH_5, BH_6, and BH_8 units were found to be the major motifs in these CaB-H compounds, and these BH_n units play a critical role in enhancing the electron-phonon coupling and the superconductivity in these compounds. The superconducting T_c values estimated using the McMillan formula are 91 and 190 K, respectively, for $R\bar{3}m$ $CaBH_6$ and $Imm2$ $CaBH_7$ compounds at 200 GPa, and 162 K for the $Fm\bar{3}m$ $CaBH_8$ phase at 300 GPa.

II. COMPUTATIONAL METHODS

Genetic algorithm (GA) search combined with first-principles density-functional theory (DFT) calculations were employed to determine the low-enthalpy structures of CaB-H_n compounds under high pressure. The unbiased global structural search based on GA method combined with first-principles structural relaxation is very effective to search a large structural phase space, which has been extensively applied to the structural prediction of crystals and clusters [31]. Candidate structures obtained from the GA search were further refined using the DFT calculations. The GA search proceeded as follows: (i) structural search started from the 60 initial random structures; (ii) using the simple cut-and-paste method, 15 offspring structures were generated at each GA generation based on the 60 parent structures; and (iii) by checking enthalpies of the 75 structures, 60 low-enthalpy structures will evolve into next generation of GA. In this work, we performed 40 generations for each GA search. In the DFT structure optimizations and total energy calculations, the Cambridge Serial Total Energy Package (CASTEP) [34] was used. The ultrasoft pseudopotentials (USP) [35] and generalized gradient approximation with Perdew-Burke-Ernzerhof [36] functional to treat exchange and correlation energy were adopted. The electron wave functions were expanded by a basis set of plane waves with an energy cutoff of 1000 eV. Monkhorst-Pack Brillouin sampling with k-point resolution of $2\pi \times 0.02$ A^{-1} was used. The convergence criterion is 0.02 meV/atom for the total energy and 0.05 eV/Å for the forces on the atoms. The phonon spectrum and electron-phonon coupling calculations were performed using the QUANTUM-ESPRESSO package [37]. USP and the plane-wave cutoff energy of 80 Ry on the kinetic energy and 800 Ry on the charge density were adopted in the calculations. The EPC parameters were calculated using 4×4×4 and 5×5×4 q-point meshes for $R\bar{3}m$ $CaBH_6$, and $Imm2$ $CaBH_7$, respectively. Denser k-point meshes, 16 × 16 × 16 and 20 × 20 × 16 for $R\bar{3}m$ $CaBH_6$ and $Imm2$ $CaBH_7$ were used for convergence checks for the EPC parameter λ.

III. RESULTS AND DISCUSSION

A. Structures

We performed the structural search for the CaB-H_n ($n =$ 1–12) at selected pressures of 50, 100, 150, 200, 250, and 300 GPa, respectively, as summarized in Fig. 1. We also adopt the $Fm\bar{3}m$ structure predicted for $LaBH_8$ by Ref. [25] and replace La with Ca to generate an $Fm\bar{3}m$ $CaBH_8$. DFT calculations show that the P_1 and Pm $CaBH_8$ are more stable in the pressure of 50–200 GPa, while the $Fm\bar{3}m$ $CaBH_8$ becomes more stable above 209 GPa (Supplemental Material, Fig. S1 [38]). The energetic stabilities of various CaB-H_n ($n = 1$–12) compounds are evaluated through their formation enthalpies with respect to the products of dissociation into CaB and solid hydrogen at 50–300 GPa, as depicted in Fig. 2. The formation enthalpy ΔH_f is given by $\Delta H_f = [H(\mathrm{CaBH}_n)\text{-}H(\mathrm{CaB})\text{-}nH(H)]/(n+2)$. The stable structures of H_2 were taken from the work of Ref. [39], and those of CaB were taken from the work of Refs. [27] and [40]. Structures with ΔH_f on the convex hull are thermodynamically stable with respect to dissociation into other structures with nearby stoichiometries, while those with ΔH_f above the convex hull are unstable or metastable. We found that the most H-rich CaB-H_n compounds with odd-H stoichiometries are more stable than those with even H stoichiometries in the whole pressure range studied. In addition to $CaBH_3$ [33] and $CaBH_5$ [33], other compounds (i.e., CaBH [33], $CaBH_2$, $CaBH_6$, $CaBH_7$, $CaBH_8$, $CaBH_9$, and $CaBH_{11}$) are also predicted to be stable under selected pressures. The most stable $CaBH_3$ and $CaBH_5$ phases lie on the convex hulls at the pressure range of 50–300 GPa. CaBH becomes stable at 100 GPa, and remains stable at 100–300 GPa. $P\bar{3}m1$ $CaBH_2$, Pm $CaBH_9$, and Cm $CaBH_{11}$ are stable at 50 GPa and in the range of 50–200 GPa, respectively. With increasing pressure, we can see that the formation enthalpies of $CaBH_6$, $CaBH_7$, and $CaBH_8$ compounds approach the convex hull from the above and land on the convex hull at 200 GPa and higher pressure. The structure parameters of the low-enthalpy CaB-H_n compounds obtained from our study are listed in Table S1.

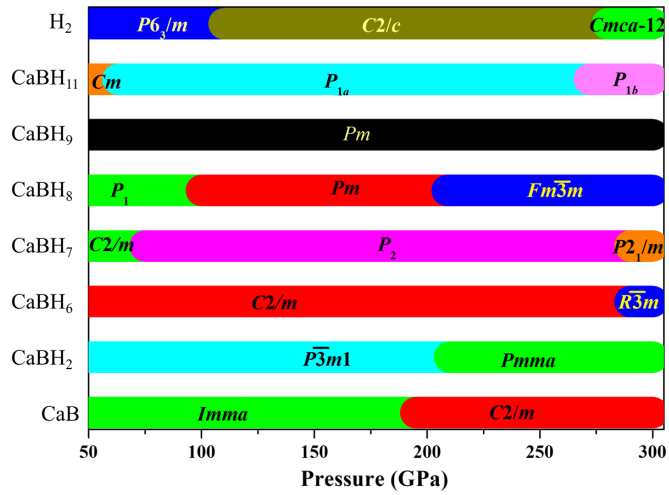

FIG. 1. Stable phases of CaB-H compounds with respect to CaB (*Imma* and $C2/m$) and H_2 ($P6_3/m$, $C2/c$, and *Cmca* 12) at the different pressures. $Fm\bar{3}m$ $CaBH_8$, CaB, and H_2 are from Refs. [25,27,39,40], respectively.

Figure 3 shows the structures of the stable and metastable CaB-H_n compounds at various pressures. $P\bar{3}m1$ $CaBH_2$ at 50 GPa [Fig. 3(a)] consists of the puckered BH layers. The

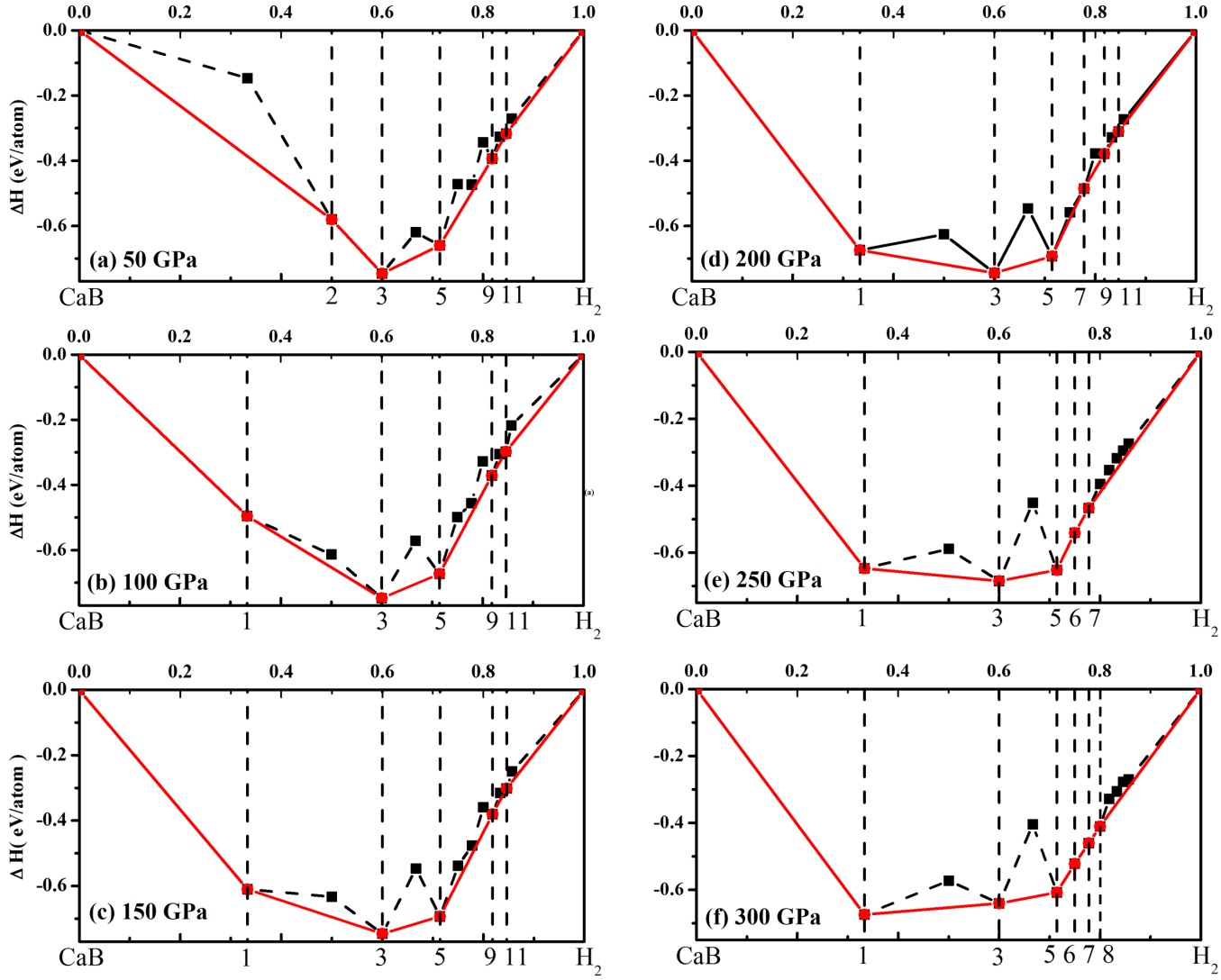

FIG. 2. Calculated formation enthalpies (in eV/atom) of CaB-H compounds with respect to CaB (*Imma* and $C2/m$) and H_2 ($P6_3/m$, $C2/c$, and *Cmca* 12) at the different pressures. $CaBH_{1,3,5}$, $CaBH_8$ ($Fm\bar{3}m$), CaB, and H_2 are from Refs. [25,27,33,39,40], respectively.

H atom and Ca atoms in the structure are accommodated between two puckered layers. As the ratio of H_n increases, quasiplanar BH_3, tetrahedral BH_4, triangular bipyramids BH_5, octahedron BH_6, and cube BH_8 motifs emerged in the CaB-H_n compounds. $CaBH_6$ is the most stable compound among those with even-H stoichiometry. In addition, $CaBH_6$ with a $C2/m$ symmetry is most stable at 50 GPa, in which the tetrahedral BH_4 and octahedron BH_6 units are intercalated with Ca atom and H_2 molecule (the H–H bond length is 0.797 Å), as shown in Fig. 3(b). As the pressure increases, the $R\bar{3}m$ phase shown in Fig. 3(c) becomes more stable for $CaBH_6$ when the pressure is above 292 GPa (Fig. S4). In the $R\bar{3}m$ structure at 300 GPa, each B atom has six H neighbors forming a B-H octahedron. As the H content further increases, tetrahedral BH_4 appears to be the major motif for $C2/m$, P_1 and P_2 $CaBH_7$ in the low pressure, as shown in Fig. 3, The BH_4 unit is separated by Ca and H atoms as well as H_2 molecule (the H–H bond length in the H_2 is 0.756, 0.787, and 0.761 Å at 50 GPa, respectively). The electron localization function from H_2 unit is about 1.0 (see Fig. 5), indicating a strong H–H covalent bond. For P_1 and P_2 $CaBH_7$ phases, transition pressures occur on 66 and 90 GPa (Fig. S6), respectively. With the pressure increasing to 263 GPa, two competitive phases appear in $CaBH_7$: one is the $P2_1/m$ phase with the BH_6 unit [Fig. 3(h)], the distance between the remaining H atom and BH_6 is only 0.982 Å at 300 GPa, the other is the $Imm2$ phase with BH_4 and H_3 unit [Fig. 3(g)], the bond length of H–H of H_3 unit is 0.951 Å at 300 GPa. At the same time, a BH_5 unit appears in P_2 phase at 300 GPa [Fig. 3(i)], which is formed by the combination of BH_4 unit and H atom. For $CaBH_8$, P_1 and Pm with BH_4 units are more stable in the pressure of 50–200 GPa, as shown in Fig. S1. With the pressure increasing to 209 GPa, $Fm\bar{3}m$ $CaBH_8$ with BH_8 motif as shown in Fig. 3(j) is most stable, in which the B–H bond length in the BH_8 unit is 1.248 Å. For $CaBH_9$, the most stable structure is the Pm structure shown in Fig. 3(k). In this $CaBH_9$ structure, tetrahedral BH_4 is still the main motif, surrounded by H_2 units and Ca atom as well as H atom. In a highly H-rich situation, $CaBH_{11}$ [Figs. 3(l)–3(n)] becomes stable in a triclinic structure (Cm) at 50 GPa and transforms to a P_{1a} phase around 63 GPa

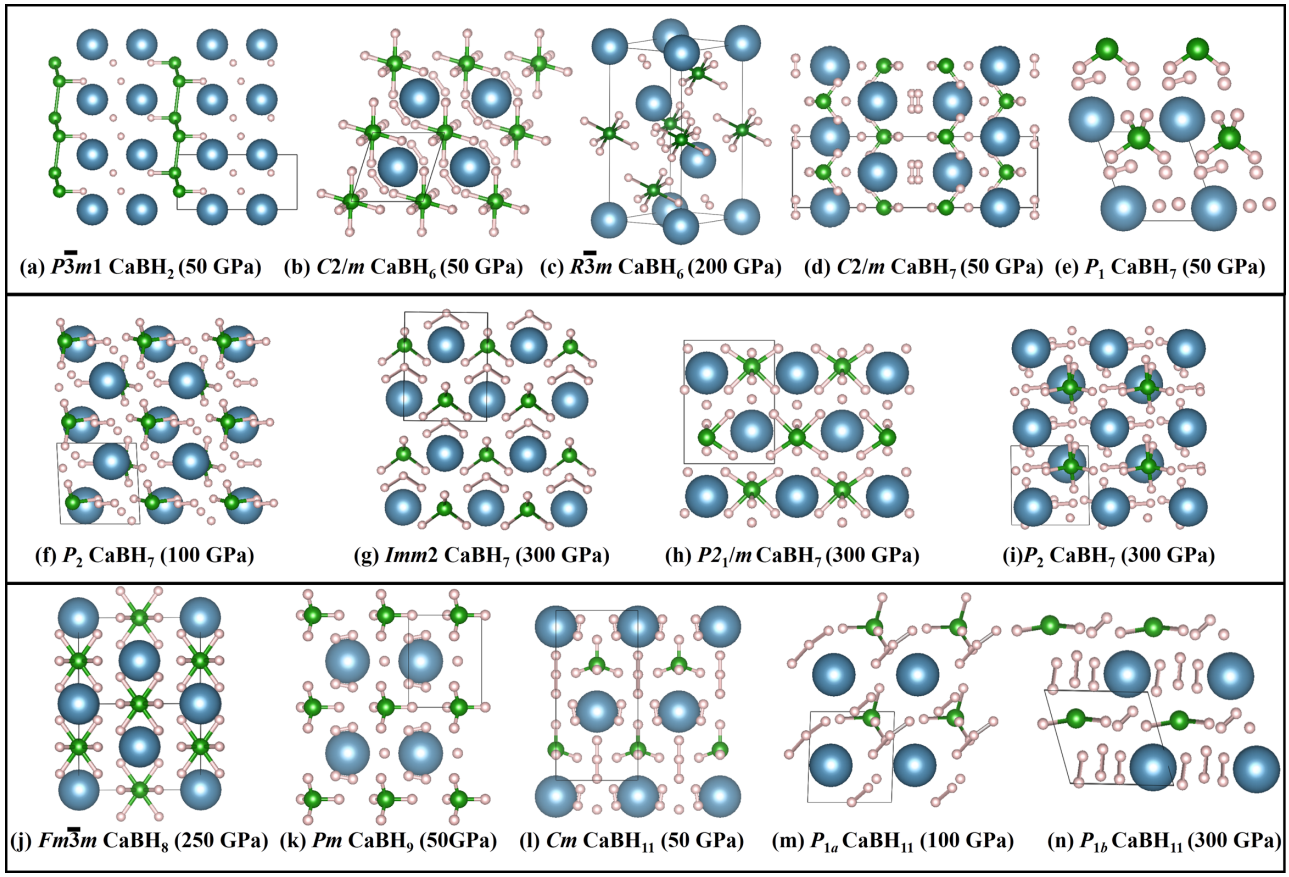

FIG. 3. Predicted crystal structures of CaB-H compounds at high pressure. (a) $P\bar{3}m1$ $CaBH_2$ at 50 GPa, (b) $C2/m$ $CaBH_6$ at 50 GPa, (c) $R\bar{3}m$ $CaBH_6$ at 200 GPa, (d) $C2/m$ $CaBH_7$ at 50 GPa, (e) P_1 $CaBH_7$ at 50 GPa, (f) P_2 $CaBH_7$ at 100 GPa, (g) $Imm2$ $CaBH_7$ at 300 GPa, (h) $P2_1/m$ $CaBH_7$ at 300 GPa, (i) P_2 $CaBH_7$ at 300 GPa, (j)$Fm\bar{3}m$ $CaBH_8$ at 250 GPa, (k) Pm $CaBH_9$, at 50 GPa, (l) Cm $CaBH_{11}$ at 50 GPa, (m) P_{1a} $CaBH_{11}$ at 100 GPa, and (n) P_{1b} $CaBH_{11}$ at 300 GPa. The blue, green, and pink spheres represent the Ca, B, and H atoms, respectively.

(Fig. S7), and then to a P_{1b} phase above 272 GPa. H_2 units and H_3 chain coexist in the Cm and P_{1a} structures of $CaBH_{11}$ under lower pressure, but only H_2 units prevail in the P_{1b} $CaBH_{11}$ under high pressure of 300 GPa. Moreover, the tetrahedral BH_4 units in the lower pressure Cm and P_{1a} structures transfer to quasiplanar BH_3 motif at 300 GPa.

We also examine the thermodynamic stability of the ternary Ca-B-H compounds at 50 and 300 GPa including the competitions from the known stable binary phases, as shown in Fig. S8. Structures located on the convex hull as shown in Fig. S8 are thermodynamically stable with respect to dissociation into other structures at nearby stoichiometries. We show that $Pa\bar{3}$ $CaBH_6$ from the Ref. [33] is about 77 meV/atom above the convex hull at 300 GPa. Although $R\bar{3}m$ $CaBH_6$ and $P2_1/m$ (or $Imm2$) $CaBH_7$ from our present search are metastable phases, the formation energies of these structures are only 10 and 12 meV/atom (or 13 meV/atom) above the convex hull at 300 GPa. These metastable compounds would be synthesized by experiment. We also proposed several possible synthesis reactions to produce $CaBH_6$ and $CaBH_7$ compounds. These synthesis reactions together with their heat of formation are listed in Table S2. Under these reaction paths, $CaBH_6$ and $CaBH_7$ always possess favorable (positive) heat of formation at 300 GPa. These energetic results for the proposed reactions provide helpful guidance to further experimental synthesis studies.

Due to the light mass of hydrogen, considering zero-point energy (ZPE) is essential for the structural stability of hydrogen-rich compound [39]. ZPE correction for the $CaBH_6$, $CaBH_7$, and $CaBH_{11}$ systems (Figs. S4, S6, and S7), as well as for CaB and H, were calculated within the quasiharmonic approximation at 50–300 GPa. As shown in Fig. S4, with considering ZPE contributions, the transition pressure reduced from 292 to 283 GPa for $C2/m$ to $R\bar{3}m$ $CaBH_6$. For $CaBH_7$ (Fig. S6), P_1, P_2, and $P2_1/m$ become stable at 67, 91, and 250 GPa, respectively. For $CaBH_{11}$ (Fig. S7), P_{1a} and P_{1b} become stable at 53 and 272 GPa, respectively. Overall, the stability of the predicted phases does not change much. Therefore, we do not consider ZPE corrections to the results presented in this paper.

B. Electronic properties

The electronic band structures and electronic densities of states (DOS) of the $CaBH_n$ compounds are calculated and shown in Fig. 4 and Figs. S9–S11, respectively. Both $C2/m$ and $R\bar{3}m$ $CaBH_6$ are good metals at 50–300 GPa. Several bands touching the Fermi level are seen in Fig. 4 for these structures at 200 GPa. These unique band dispersion

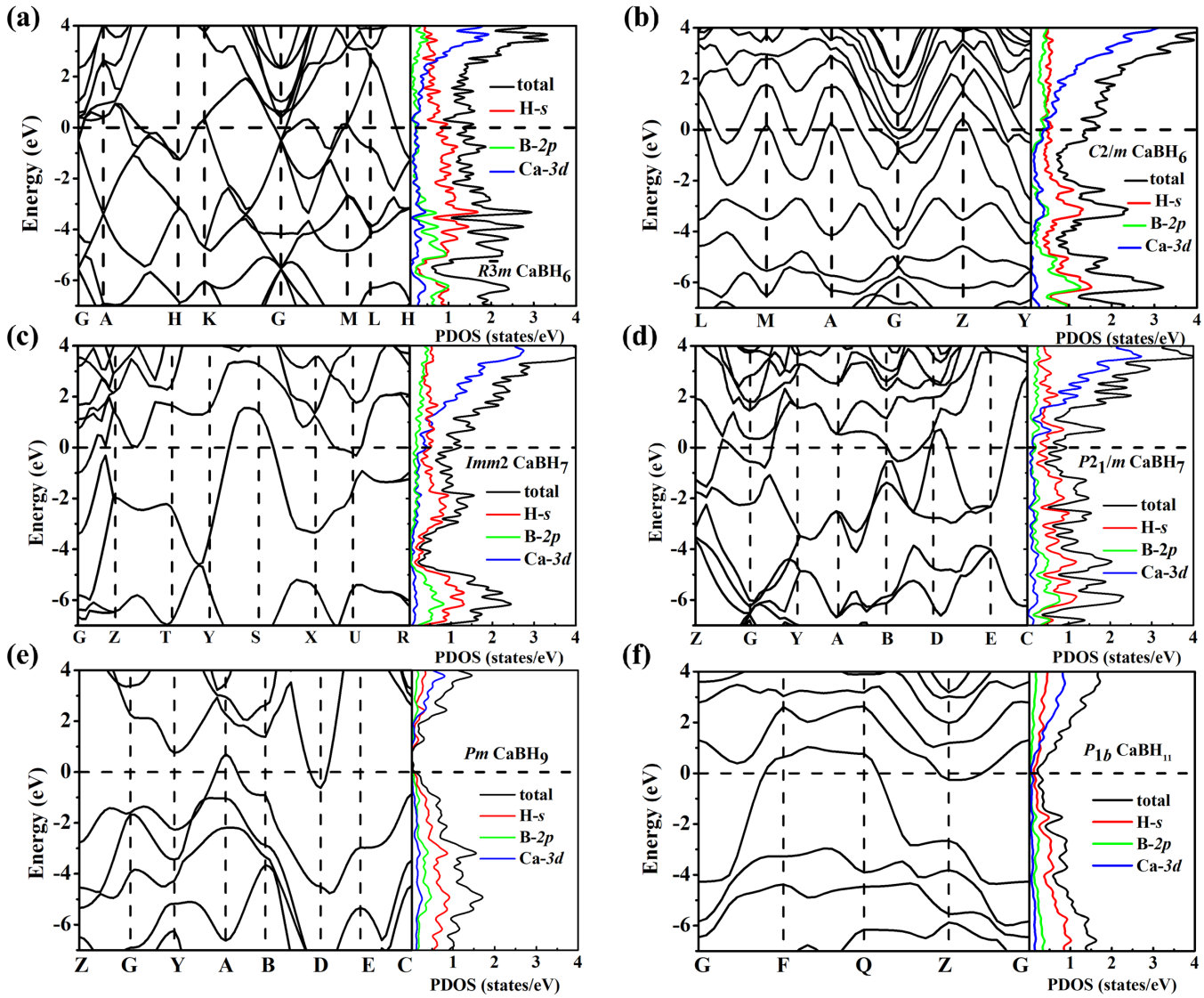

FIG. 4. Electronic band structures and density of states of CaB-H compounds. (a) $R\bar{3}m$ $CaBH_6$ at 200 GPa, (b) $C2/m$ $CaBH_6$ at 200 GPa, (c) $Imm2$ $CaBH_7$ at 200 GPa, (d) $P2_1/m$ $CaBH_7$ at 200 GPa, (e) Pm $CaBH_9$, at 250 GPa, and (f) P_{1b} $CaBH_{11}$ at 300 GPa.

contribute larger DOS around the Fermi level which is beneficial to enhancing the superconductivity of the compounds. For $CaBH_7$, $C2/m$ at 50 GPa and P_2 phase at 100–250 GPa are semiconducting with band gaps of 1.192 eV and 0.614–0.350 eV (Fig. S9), respectively. Therefore, these compounds do not exhibit superconductivity below 250 GPa. At 300 GPa, the band of P_2 $CaBH_7$ compound crosses the Fermi level along the *G-F* and *Z-G* directions, leading to a metallic feature (Fig. S9). By contrast, $Imm2$ and $P2_1/m$ $CaBH_7$ exhibit strong metallic features as can be seen from Figs. 4(c) and 4(d), respectively. Higher electronic DOS near the Fermi energy level contributes to the relative high superconducting T_c of these two compounds (see Table I). From the local DOS analysis, we see that the H-1 *s* state provides the largest contribution to the DOS near the Fermi level (especially for the $R\bar{3}m$ $CaBH_6$) as shown in Fig. 4.

We also found that Pm $CaBH_9$, and P_{1b} $CaBH_{11}$ display semiconducting character with indirect band gaps which change from 1.633 to 0.144 eV in Pm $CaBH_9$ and from 2.474 to 0.122 eV in P_{1b} $CaBH_{11}$ when the presses increase from 50 to 200 GPa (Figs. S10 and S11), respectively. For $CaBH_9$, the band dispersion crosses the Fermi level at the *A* point as shown in Fig. 4(e), leading to a weak metallic state when the pressure is above 200 GPa. However, the DOS at the Fermi level is too small to lead to any significant superconductivity. For $CaBH_{11}$ at 300 GPa, one narrow band crosses the Fermi level near the *F* and *Q* points and lays about 1 eV above the Fermi level between these two *K* points so it contributes very little to the DOS at the Fermi level. Surprisingly, the superconducting T_c of this compound above 250 GPa is significant (about 120 K, see Table I) although the DOS at the Fermi level is not high. This would be due to the strong electron-phonon coupling strength in this system.

We also calculated the electron localization functions (ELF) for ternary $CaBH_6$ and $CaBH_7$ compounds. As shown in Fig. 5, the ELF values of B-H in BH_6 or BH_4 units in CaB-H ($n = 6$ and 7) are $0.65 \sim 0.75$, indicating their covalent characters. The ELF values of H-H in H_2 and H_3 units for

TABLE I. Calculated electron-phonon coupling parameters (λ), the logarithmic average phonon frequency $\omega_{\log}$(K), electronic density of states at the Fermi level $N(E_f)$ (in states/Ry), and superconducting critical temperatures T_c (K) for the CaB-H compounds at selected pressures.

Structure	Space group	Pressure (GPa)	λ	$N(E_f)$	$\omega_{\log}$	T_c (K) $\mu = 0.13 \sim 0.1$
$CaBH_2$	$P\bar{3}m1$	100	0.20	2.28	1158	0
	P_3	50	1.01	4.77	752	46–53
	$R\bar{3}m$	200	0.94	9.14	1467	76–91
		250	0.92	9.08	1585	80–95
$CaBH_6$		300	0.91	9.07	1631	83–98
	$C2/m$	100	0.98	10.25	825	48–56
		200	1.02	9.76	1057	67–76
		300	1.12	9.44	1168	84–96
	$Imm2$	200	2.80	6.76	822	184–190
		250	2.14	6.85	1026	168–184
		300	2.22	7.05	1062	183–200
$CaBH_7$	$P2_1/m$	150	1.34	6.08	1286	117–135
		200	1.69	6.11	1025	136–151
		300	1.29	6.33	1380	121–135
	P_2	300	1.64	6.54	954	123–136
$CaBH_8$	Pm	150	0.86	2.80	1037	46–55
		200	0.99	2.73	1076	63–74
	$Fm\bar{3}m$	250	1.44	3.88	1524	152–167
		300	1.31	3.74	1635	146–162
$CaBH_9$	Pm	250	0.20	0.55	1046	0
		300	0.36	0.91	905	1–2
$CaBH_{11}$	P_{1b}	250	1.75	3.73	822	112–123
		300	1.60	3.91	937	112–128

these structures are very high (close to 1), indicating that they are strong covalent bond. While the ELF values for the Ca atoms are close to 0, implying that Ca–H is ionic bond. The Bader charge calculation shows the Ca atoms in the $CaBH_6$ ($R\bar{3}m$ and $C2/m$) and $CaBH_7$ ($Imm2$ and $P2_1/m$) act as electron donors, which donate 1.39e/1.42e and 1.41e/1.46e at 300 GPa, BH_4, BH_6, and H_2 (or H_3) units are acceptors.

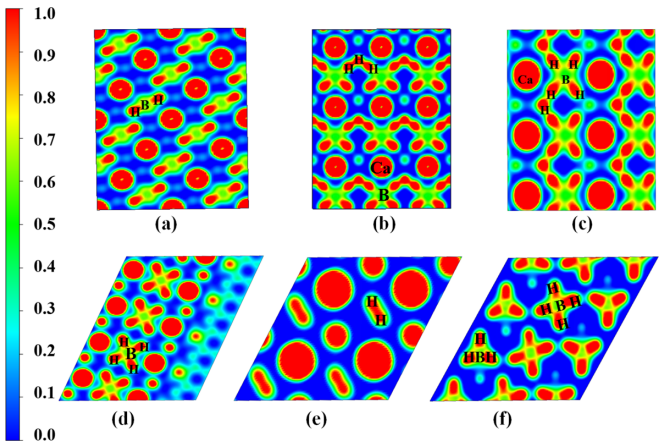

FIG. 5. 2D-ELF of CaB-H compounds. (a), (d) $R\bar{3}m$ $CaBH_6$ on the (110) and $(0\bar{1}3)$ planes, respectively, (b) $Imm2$ $CaBH_7$ on the (100) plane, (c) $P2_1/m$ $CaBH_7$ on the (001) plane, and (e), (f) $C2/m$ $CaBH_6$ on the (001) and (010) planes, respectively.

C. Superconducting properties

We also explore possible superconductivity in the CaB-H compounds at different pressure by calculating the logarithmic average phone frequency $\omega_{\log}$, the electron-phonon coupling parameter λ, and the electronic DOS at the Fermi level, $N(E_f)$ (Table I). For Pm $CaBH_9$, at 250 GPa, $\omega_{\log}$ is 1046 K and the λ is only 0.16. The small value of λ makes the T_c in $CaBH_9$ close to 0 K. By contrast, the calculated λ and $\omega_{\log}$ values are 0.94 (1.02) and 1467 K (1057 K) for $R\bar{3}m$ $CaBH_6$ (or $C2/m$) at 200 GPa, the correspondingly T_c values are 76–91 K (67–76 K) according to the McMillan equation. We also performed phonon and EPC calculations for the Pm and the $Fm\bar{3}m$ $CaBH_8$. The calculated EPC parameters, λ, for the Pm at 200 GPa and $Fm\bar{3}m$ at 300 GPa are 0.99 and 1.31, respectively, which give T_c values of 63–74 and 146–162 K, respectively. The EPC parameter λ is larger than 1.5, which represents very strong electron-phonon coupling for systems. The McMillan equation [45] needs to be corrected by including two correction factors f_1 and f_2, $T_c = \frac{f_1 f_2 \omega_{\log}}{1.20} \exp[\frac{-1.04(1+\lambda)}{\lambda(1-0.62\mu^*)-\mu^*}]$, which represent the strong coupling and the shape correction, respectively. In our work, for the $Imm2$ and $P2_1/m$ $CaBH_7$ at 200 GPa and P_{1b} $CaBH_{11}$ at 300 GPa, the EPC parameters λ are much higher than the other CaB-H ternary compounds, which are 2.80, 1.69, and 1.75, respectively. The final corrected T_c values are about 184–190 K, 136–151 K, for $Imm2$ and $P2_1/m$ $CaBH_7$ at 200 GPa, and 112–128 K for P_{1b} $CaBH_{11}$ at 300 GPa, respectively.

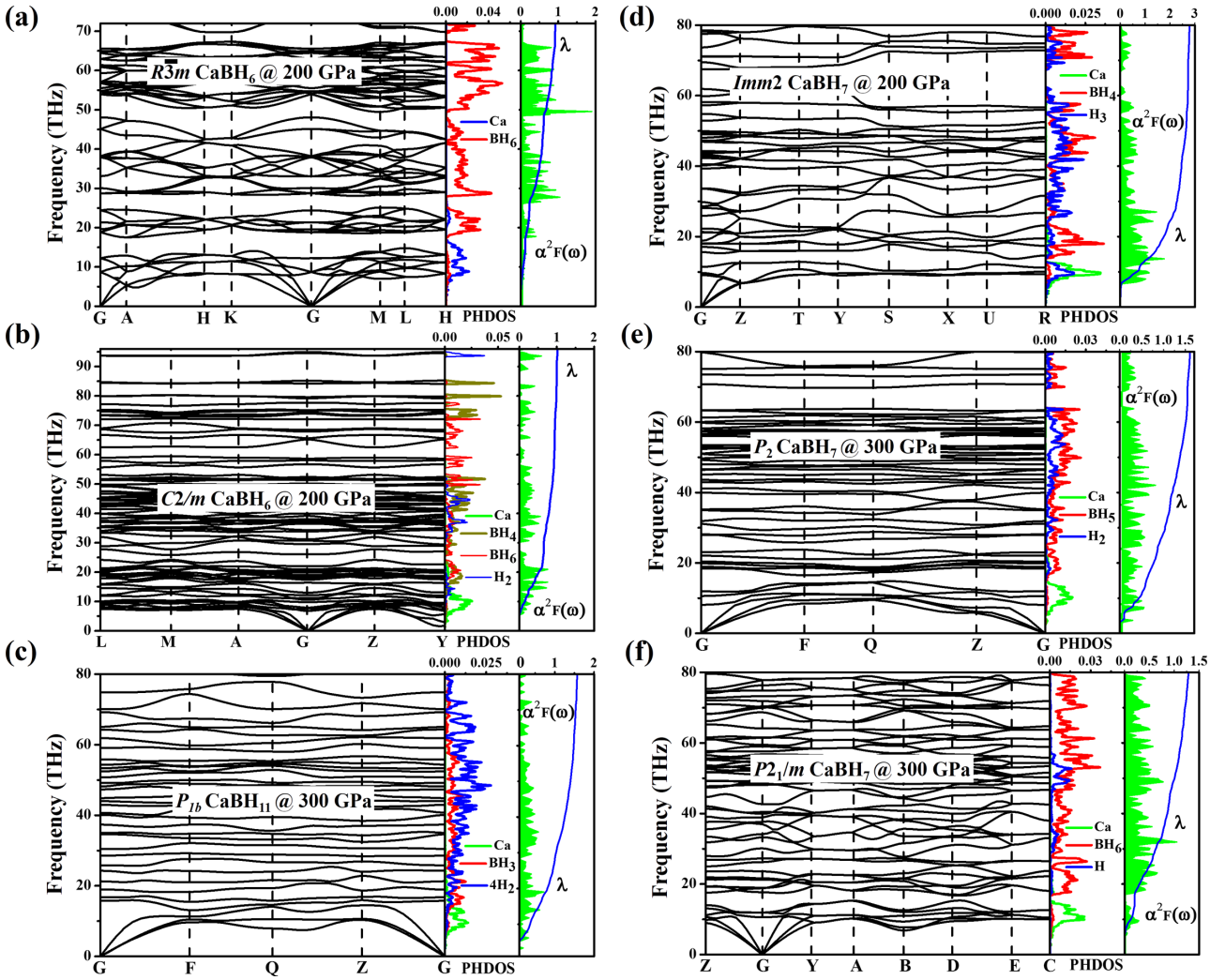

FIG. 6. Calculated phonon band structures, phonon density of states, the Eliashberg phonon spectral function, $\alpha^2F(\omega)$, and the partial electron-phonon intergral, $\lambda(\omega)$ for CaB-H compounds. (a) $R\bar{3}m$ $CaBH_6$ at 200 GPa, (b) $C2/m$ $CaBH_6$ at 200 GPa, (c) P_{1b} $CaBH_{11}$ at 300 GPa, (d) $Imm2$ $CaBH_7$ at 200 GPa, (e) P_2 $CaBH_7$ at 300 GPa, and (f) $P2_1/m$ $CaBH_7$ at 300 GPa.

Figure 6 show the phonon dispersions and the projected phonon density of states, Eliashberg spectral function $\alpha^2F(\omega)$, and the electron-phonon coupling integral, $\lambda(\omega)$ for CaB-H compounds. We found that the electron-phonon coupling of CaB-H compounds is mainly from hydrogen–boron bonding within the BH_n units. For $C2/m$ and $R\bar{3}m$ $CaBH_6$, there is no imaginary frequency in the phonon dispersion curves under the given pressures, suggesting the dynamical stability of these compounds. For $R\bar{3}m$ $CaBH_6$, vibrations of Ca atom (below 15 THz) contribute 14% of the total λ, whereas the remaining 86% comes from vibration modes of BH_6 unit. Similarly, the B-H vibration modes of BH_4 and BH_6 units from $C2/m$ $CaBH_6$ also donate about 60% of the total λ. For P_{1b} $CaBH_{11}$, the optical modes are mainly from the Ca atom. The low-frequency (below 14 THz) modes are associated with Ca atom, which contribute about 31% of the total λ. The intermediate frequencies (between 14 and 18 THz) come mainly from the vibrations of quasiplanar BH_3 unit, including a small amount vibration modes of Ca atom and H_2 units, which contribute only 13% of the total λ. The frequency intervals greater than 18 THz are origin from the B-H modes of BH_3 unit and H-H modes of molecular H_2 units, which contribute 56% of total λ.

Due to the strong electron-phonon coupling, the $Imm2$ $CaBH_7$ has a high T_c, which value is about 184–190 K at 200 GPa. At 200 GPa (Fig. 6), the low-frequency vibration modes (below 13 THz) are mainly from the vibrations of Ca atom and H_3 unit, with some amount of vibration intensity from the tetrahedral BH_4 unit, which contribute about 33% of total λ. The high-frequency modes (>24 THz) are originated from the BH_4 and H_3 units, which contribute 29% of λ. The intermediate frequency bands (between 13 and 24 THz) are originated from the vibrations of the tetrahedral BH_4, which contribute about 38% of the total value of λ. As pressure increases to 250 (or 300 GPa), the calculated $\omega_{\log}$ for the $Imm2$ $CaBH_7$ increases to 1026 K (or 1062 K), $N(E_f)$ increases to 6.85 (or 7.05). The responsible λ is 2.14 (or 2.22), which indicates the strong electron-phonon coupling. And, we found that the contribute of the B-H vibration modes from BH_4 unit to the total λ increases to 48% at 250 GPa and 52% at 300 GPa, respectively. Similarly, we also found that BH_5 and BH_6 units play an important role for EPC of P_2 and $P2_1/m$ $CaBH_7$,

as shown in Figs. 6(e) and 6(f). BH_4, BH_5, and BH_6 units are the major units in the $Imm2$, P_2, and $P2_1/m$ phases of $CaBH_7$ at 300 GPa. We found that when the number of H atoms in the BH_n unit increases from 4 to 6 in the $Imm2$ to the $P2_1/m$ phases, the corresponding EPC parameter λ decreases from 2.22 to 1.29. This observation suggest that although BH_n units in $CaBH_7$ compounds are essential for achieving superconductivity, too many H atoms in a BH_n unit may reduce the strength of the EPC parameter λ in $CaBH_7$, and thus reduce the superconducting T_c.

IV. CONCLUSIONS

In summary, we have explored the crystal structures and electron properties of the H-rich CaB-H_n compounds under high pressure by GA search in combination with first-principles DFT calculations. The results showed that the H-rich $CaBH_n$ compound with odd-H stoichiometry (e.g., $CaBH_7$, $CaBH_9$, and $CaBH_{11}$) is more stable. $CaBH_6$ and $CaBH_8$ are the stable compounds with the even-H stoichiometry. BH_3, BH_4, BH_5, BH_6, and BH_8 units were found to be the major motifs in these CaB-H compounds. Among these compounds, metastable phase $Imm2$ from $CaBH_7$ was found to be dynamically stable above 180 GPa, and it exhibits strong electron-phonon coupling which drives the superconducting T_c up to ∼200 K at 200 GPa. The high T_c in this compound is closely related to the strong electron-phonon coupling, which is mainly from hydrogen-boron bonding within the BH_4 unit. Our results will provide guidance for the experimental work on discovery of novel superconductor in CaB-H compounds.

ACKNOWLEDGMENTS

This work was supported by the National Natural Science Foundation of China (Grants No. 21773132, No. 12004210, and No. 21603114); Natural Science Foundation of Shandong Province (Grant No. ZR2020MB046); the Higher Educational Science and Technology Program of Shandong Province of China (Grant No. J17KA179). Work at Ames Laboratory was supported by the U.S. Department of Energy (DOE), Office of Science, Basic Energy Sciences, Materials Science and Engineering Division including a grant of computer time at the National Energy Research Scientific Computing Centre (NERSC) in Berkeley, CA. Ames Laboratory is operated for the U.S. DOE by Iowa State University under Contract No. DE-AC02-07CH11358.

[1] C. Narayana, H. Luo, J. Orloff, and A. L. Ruoff, Nature (London) **393**, 46 (1998).
[2] N. W. Ashcroft, Phys. Rev. Lett. **92**, 187002 (2004).
[3] E. Snider, N. Dasenbrock-Gammon, R. McBride, M. Debessai, H. Vindana, K. Vencatasamy, K. V. Lawler, A. Salamat, and R. P. Dias, Nature (London) **586**, 373 (2020).
[4] A. P. Drozdov, M. I. Eremets, I. A. Troyan, V. Ksenofontov, and S. I. Shylin, Nature (London) **525**, 73 (2015).
[5] D. F. Duan, Y. X. Liu, F. B. Tian, D. Li, X. L. Huang, Z. L. Zhao, H. Y. Yu, B. B. Liu, W. J. Tian, and T. Cui, Sci. Rep. **4**, 6968 (2014).
[6] D. F. Duan, X. L. Huang, F. B. Tian, D. Li, H. Y. Yu, Y. X. Liu, Y. B. Ma, B. B. Liu, and T. Cui, Phys. Rev. B **91**, 180502 (2015).
[7] A. P. Drozdov, P. P. Kong, V. S. Minkov, S. P. Besedin, M. A. Kuzovnikov, S. Mozaffari, L. Balicas, F. F. Balakirev, D. E. Graf, and V. B. Prakapenka, E. Greenberg, D. A. Knyazev, and M. Tkacz, Nature (London) **569**, 528 (2019).
[8] M. Somayazulu, M. Ahart, A. K. Mishra, Z. M. Geballe, M. Baldini, Y. Meng, V. V. Struzhkin, and R. J. Hemley, Phys. Rev. Lett. **122**, 027001 (2019).
[9] X. L. Feng, J. R. Zhang, G. Y. Gao, H. Y. Liu, and H. Wang, RSC Adv. **5**, 59292 (2015).
[10] H. Wang, J. S. Tse, K. Tanaka, T. Iitaka, and Y. M. Ma, Proc. Natl. Acad. Sci. USA **109**, 6463 (2012).
[11] H. Y. Liu, I. I. Naumov, R. Hoffmann, N. W. Ashcroft, and R. J. Hemley, Proc. Natl. Acad. Sci. USA **114**, 6990 (2017).
[12] F. Peng, Y. Sun, C. J. Pickard, R. J. Needs, Q. Wu, and Y. Ma, Phys. Rev. Lett. **119**, 107001 (2017).
[13] D. Z. Meng, M. Sakata, K. Shimizu, Y. Iijima, H. Saitoh, and T. Sato, Phys. Rev. B **99**, 024508 (2019).
[14] M. Rahm, R. Hoffmann, and N. W. Ashcroft, J. Am. Chem. Soc. **139**, 8740 (2017).
[15] S. T. Zhang, L. T. Zhu, H. Y. Liu, and G. C. Yang, Inorg. Chem. **55**, 11434 (2016).
[16] Y. B. Ma, D. F. Duan, Z. J. Shao, H. Y. Yu, H. Liu, F. B. Tian, X. L. Huang, D. Li, B. B. Liu, and T. Cui, Phys. Rev. B **96**, 144518 (2017).
[17] Y. B. Ma, D. F. Duan, Z. J. Shao, D. Li, L. Y. Wang, H. Y. Yu, F. B. Tian, H. Xie, B. B. Liu, and T. Cui, Phys. Chem. Chem. Phys. **19**, 27406 (2017).
[18] X. W. Liang, A. Bergara, L. Y. Wang, B. Wen, Z. S. Zhao, X. F. Zhou, J. L. He, G. Y. Gao, and Y. J. Tian, Phys. Rev. B **99**, 100505 (2019).
[19] Da. Li, Y. Liu, F. B. Tian, S. L. Wei, Z. Liu, D. F. Duan, B. B. Liu, and T. Cui, Front. Phys. **13**, 137107 (2018).
[20] X. W. Liang,S. T. Zhao, C. C. Shao, A. Bergara, H. Y. Liu, L. Y. Wang, and R. X. Sun, Phys. Rev. B **100**, 184502 (2019).
[21] X. Du, S. T. Zhang, J. Y. Lin, X. H. Zhang, A. Bergaram, and G. C. Yang, Phys. Rev. B **100**, 134110 (2019).
[22] C. Kokail, W. Linden, and L. Boeri, Phys. Rev. Mater **1**, 074803 (2017).
[23] Y. Sun, J. Lv, Y. Xe, H. Y. Lu, and Y. M. Ma, Phys. Rev. Lett. **123**, 097001 (2019).
[24] S. D. Catado, C. Heil, W. Linden, and L. Boeri, Phys. Rev. B **104**, L020511 (2021).
[25] X. W. Liang, A. Bergara, X. D. Wei, L. Y. Wang, R. X. Sun, H. Y. Liu, R. J. Hemley, L. Wang, G. Y. Gao, and Y. J. Tian, Phys. Rev. B **104**, 134501 (2021).
[26] S. D. Cataldo, W. Linden, and L. Boeri, arXiv:2106.07266.
[27] S. Shah and A. N. Kolmogorov, Phys. Rev. B **88**, 014107 (2013).
[28] H. J. Choi, S. G. Louie, and M. L. Cohen, Phys. Rev. B **80**, 064503 (2009).
[29] Y. Yao and R. Hoffmann, J. Am. Chem. Soc. **133**, 21002 (2011).
[30] C. H. Hu, A. R. Oganov, Q. Zhu, G. R. Qian, G. Frapper, A. O. Lyakhov, and H. Y. Zhou, Phys. Rev. Lett. **110**, 165504 (2013).

[31] W. H. Yang, W. C. Lu, S. D. Li, X. Y. Xue, Q. J. Zang, K. M. Ho, and C. Z. Wang, Phys. Chem. Chem. Phys. **21**, 5466 (2019).

[32] Z. J. Shao, D. F. Duan, Y. B. Ma, H. Y. Yu, H. Song, H. Xie, D. Li, F. B. Tian, B. B. Liu, and T. Cui, Inorg. Chem. **58**, 2558 (2019).

[33] S. D. Catakdi, W. Linden, and L. Boeri, Phys. Rev. B **102**, 014516(2020).

[34] V. Milman, B. Winkler, J. A. White, C. J. Pickard, M. C. Payne, E. V. Akhmatskaya, and R. H. Nobes, Int. J. Quantum Chem. **77**, 895 (2000).

[35] D. Vanderbilt, Phys. Rev. B **41**, 7892 (1990).

[36] J. P. Perdew, K. Burke, and M. Ernzerhof, Phys. Rev. Lett. **77**, 3865 (1996).

[37] P. Giannozzi, S. Baroni, N. Bonini, M. Calandra, R. Car, C. Cavazzoni, G. L. Chiarotti, M. Cococcioni, I. Dabo, A. Dal Corso *et al.*, J. Phys.: Condens. Matter **21**, 395502 (2009).

[38] See Supplemental Material at http://link.aps.org/supplemental/10.1103/PhysRevB.104.174106 for crystal structure information, calculated formation enthalpy, electronic band structures and phonon dispersions, 2D-ELF and ternary phase diagram for all predicted CaB-H compounds, which includes Refs. [10,25,27–31,39–44].

[39] C. J. Pickard and R. J. Needs, Nat. Phys. **3**, 473 (2007).

[40] At the pressure of 50 GPa, CaB is found to be stable with *Imma* symmetry [27]. Under high pressure, we performed the structural search for the CaB at selected pressures of 100, 150, 200, 250, and 300 GPa, respectively; we found that *Imma* CaB still retains stable until 195 GPa and $C2/m$ CaB becomes stable above 195 GPa. The corresponding structural information are given in Table S1.

[41] J. S. Tse, D. D. Klug, S. Desgreniers, J. S. Smith, R. Flacau, Z. Liu, J. Hu, N. Chen, and D. T. Jiang, Phys. Rev. B **75**, 134108 (2007).

[42] Y. W. Li, B. Li, T. Cui, Y. Li, L. J. Zhang, Y. M. Ma, and G. T. Zou, J. Phys.: Condens. Matter **20**, 045211 (2008).

[43] A. R. Oganov, J. H. Chen, C. Gatti, Y. Z. Ma, Y. M. Ma, C. W. Glass, Z. X. Liu, T. Yu, O. O. Kurakevych, and V. L. Solozhenko, Nature (London) **457**, 863 (2009).

[44] Y Yao, D. D Klug, J. Sun, and M. Marto, Phys. Rev. Lett. **103**, 055503 (2009).

[45] P. B. Allen and R. Dynes, Phys. Rev. B **12**, 905 (1975).